Letter

Birational transformations on dimer integrable systems

Minsung Kho[*]
Department of Mathematical Sciences, Ulsan National Institute of Science and Technology, 50 UNIST-gil, Ulsan 44919, South Korea

Norton Lee[†]
Center for Geometry and Physics, Institute for Basic Science (IBS), Pohang 37673, South Korea

Rak-Kyeong Seong[‡]
Department of Mathematical Sciences, and Department of Physics, Ulsan National Institute of Science and Technology, 50 UNIST-gil, Ulsan 44919, South Korea

(Received 30 April 2025; accepted 16 July 2025; published 4 August 2025)

We show that when two toric Calabi-Yau 3-folds and their corresponding toric varieties are related by a birational transformation, they are associated with a pair of dimer models on the 2-torus that define dimer integrable systems, which themselves become birationally equivalent. Under this birational equivalence, the Casimirs and the Hamiltonias as well as the spectral curve and the Poisson structure formed by the cluster variables of the dimer integrable systems are identified to each other. These integrable systems defined by dimer models were first introduced by Goncharov and Kenyon. We illustrate this equivalence explicitly using a pair of dimer integrable systems corresponding to the Abelian orbifolds of the form $\mathbb{C}^3/\mathbb{Z}_4 \times \mathbb{Z}_2$ with orbifold action (1, 0, 3)(0, 1, 1) and $\mathcal{C}/\mathbb{Z}_2 \times \mathbb{Z}_2$ with action (1, 0, 0, 1)(0, 1, 1, 0), whose spectral curves and Hamiltonians are shown to be related by a birational transformation.

DOI: 10.1103/1mll-95cs

Birational geometry focuses on classifying algebraic varieties up to birational equivalence and has profoundly impacted our understanding of algebraic varieties, particularly through the minimal model program (MMP) initiated by Mori [1–3] and through subsequent developments [4–13]. More recently, it has been argued that such birational transformations also connect supersymmetric gauge theories realized in string theory [14,15]. In particular, when a D3-brane probes a toric Calabi-Yau 3-fold, its worldvolume theory is a $4d$ $\mathcal{N}=1$ supersymmetric quiver gauge theory, which is encoded in a bipartite graph on a 2-torus also known as a dimer model [16,17] or a brane tiling [18–20]. It can be shown that if two such $4d$ $\mathcal{N}=1$ theories are related by a mass deformation [21–24], then the toric varieties of the associated toric Calabi-Yau 3-folds are related by a birational transformation [8,14,15,25].

These birational transformations act on Newton polynomials of the form,

$$P(x,y) = \sum_{(n_x,n_y)\in\Delta} c_{(n_x,n_y)} x^{n_x} y^{n_y}, \tag{1}$$

where $x, y \in \mathbb{C}^*$ and $(n_x, n_y) \in \mathbb{Z}^2$ are coordinates of points in the toric diagram Δ, which characterizes the toric variety $X(\Delta)$ [26,27]. The Newton polynomial is also given by the permanent of the Kasteleyn matrix K of the dimer model, $P(x,y) = \mathrm{perm}(K)$ [17,28]. The birational transformations φ_A act on $P(x,y)$ as follows:

$$\varphi_A : (x,y) \mapsto (A(y)x, y), \tag{2}$$

where the Laurent polynomial $A(y)$ is chosen to be such that $A(y)^{-m}$ is a polynomial divisor of $C_m(y)$ for $a \le m \le -1$ in the expansion $P(x,y) = \sum_{m=a}^{b} C_m(y)x^m$. Here, $a<0$ and $b>0$ and $C_m(y)$ are subpolynomials for $a \le m \le b$. We identify the corresponding toric varieties as birationally equivalent, if the birational map in (2) applies for at least one chosen $GL(2,\mathbb{Z})$ frame or choice of origin in $\mathbb{Z}^2$ for the toric diagrams Δ.

As shown by Goncharov and Kenyon [29,30], a dimer model realized as a bipartite graph on T^2 gives rise to an

[*]Contact author: minsung@unist.ac.kr
[†]Contact author: norton.lee@ibs.re.kr
[‡]Contact author: seong@unist.ac.kr

integrable system [30–35], where the spectral curve is given by the zero locus,

$$\Sigma: P(x, y) = 0. \tag{3}$$

This holomorphic curve also plays an essential role in the type IIB brane configuration consisting of a D5-brane suspended between an NS5-brane wrapping Σ, which is represented by the bipartite graph of the dimer model and is T-dual to the D3-brane probing the toric Calabi-Yau 3-fold [36–39]. Σ is also known as the mirror curve of the mirror Calabi-Yau 3-fold [40–42].

In this work, we discover for the first time that the integrable systems defined by two dimer models, whose toric Calabi-Yau 3-folds are related by a birational transformation as given in (2), are identical up to a redefinition of parameters corresponding to zigzag paths and face loops in the dimer models. We illustrate this discovery with an explicit example based on the dimer models corresponding to the abelian orbifold of the form $\mathbb{C}^3/\mathbb{Z}_4 \times \mathbb{Z}_2$ with orbifold action (1, 0, 3)(0, 1, 1) [43,44], also referred to as model 2 in the classification of [45], and toric phase a of the Abelian orbifold of the form $\mathcal{C}/\mathbb{Z}_2 \times \mathbb{Z}_2$ with action (1, 0, 0, 1)(0, 1, 1, 0), also referred to as phase a of PdP_5 [19,46] and model 4a in [45].

Dimer integrable systems. A perfect matching p_a is a set of edges $e_{ij} = (w_i, b_j)$ in the dimer model, such that edges in p_a connect to all white nodes w_i and black nodes b_i uniquely once. These perfect matchings play an important role as GLSM fields [47] that parametrize the associated toric Calabi-Yau 3-fold. We define the weight $\bar{p}_a$ of a perfect matching p_a as the product,

$$\bar{p}_a = \prod_{e_{ij} \in p_a} e_{ij}^{+}, \qquad (\bar{p}_a)^{-1} = \prod_{e_{ij} \in p_a} e_{ij}^{-}, \tag{4}$$

where we introduce directed edges defined as e_{ij}^{+}: $w_i \to b_j$ and e_{ij}^{-}: $b_j \to w_i$. Here, the positive sign indicates an edge directed from a white node w_i to a black node b_j, and the negative sign indicates the same edge but in the opposite direction. With this convention, we define the following product of perfect matching weights:

$$\bar{p}_a \cdot (\bar{p}_b)^{-1} \equiv \cdots e_{ij}^{+} e_{kj}^{-} e_{kl}^{+} e_{ml}^{-} \cdots, \tag{5}$$

where $\bar{p}_a = \cdots e_{ij}^{+} e_{kl}^{+} \cdots$ and $(\bar{p}_b)^{-1} = \cdots e_{kj}^{-} e_{ml}^{-} \cdots$. This product yields an ordered sign-alternating sequence of directed edge variables corresponding to a path in the dimer.

All closed connected and directed paths composed of sign-alternating edges $e_{ij}^{\pm}$ in a dimer model on T^2 can be expressed as permutation tuples of the permutation group S_{2n_e}, where n_e is the number of edges in the dimer model

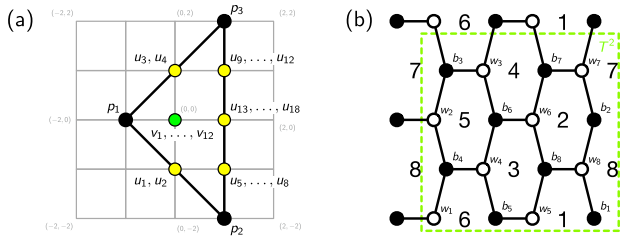

FIG. 1. (a) The toric diagram and (b) the dimer model for $\mathbb{C}^3/\mathbb{Z}_4 \times \mathbb{Z}_2$ (1, 0, 3)(0, 1, 1) [model 2]. Points in the toric diagram are labeled by corresponding perfect matchings in the dimer model.

[48,49]. Given two such permutation tuples, we can define the following product:

$$\begin{aligned}&(\cdots e_{ik}^{-} e_{ij}^{+} e_{mj}^{-} \cdots)(\cdots e_{uj}^{+} e_{ij}^{-} e_{iv}^{+} \cdots) \\ &\quad = (\cdots e_{ik}^{-} e_{iv}^{+} \cdots)(\cdots e_{uj}^{+} e_{mj}^{-} \cdots),\end{aligned} \tag{6}$$

giving a new pair of closed paths with the identities $(e_{ij}^{\pm})^{-1} = e_{ij}^{\mp}$ and $e_{ij}^{+} e_{ij}^{-} = 1$.

Model 2: $\mathbb{C}^3/\mathbb{Z}_4 \times \mathbb{Z}_2$ (1, 0, 3)(0, 1, 1): The dimer model, referred to here as model 2, corresponding to the abelian orbifold of the form $\mathbb{C}^3/\mathbb{Z}_4 \times \mathbb{Z}_2$ with orbifold action (1, 0, 3)(0, 1, 1) is shown in Fig. 1(b) with a choice of a fundamental domain on T^2. The corresponding Kasteleyn matrix takes the following form:

$$K = \begin{array}{c|cccccccc} & b_1 & b_2 & b_3 & b_4 & b_5 & b_6 & b_7 & b_8 \\ \hline w_1 & e_{11}x^{-1} & 0 & e_{13}y^{-1} & e_{14} & 0 & 0 & 0 & 0 \\ w_2. & 0 & e_{22}x^{-1} & e_{23} & e_{24} & 0 & 0 & 0 & 0 \\ w_3 & 0 & 0 & e_{33} & 0 & e_{35}y & e_{36} & 0 & 0 \\ w_4 & 0 & 0 & 0 & e_{44} & e_{45} & e_{46} & 0 & 0 \\ w_5 & 0 & 0 & 0 & 0 & e_{55} & 0 & e_{57}y^{-1} & e_{58} \\ w_6 & 0 & 0 & 0 & 0 & 0 & e_{66} & e_{67} & e_{68} \\ w_7 & e_{71}y & e_{72} & 0 & 0 & 0 & 0 & e_{77} & 0 \\ w_8 & e_{81} & e_{82} & 0 & 0 & 0 & 0 & 0 & e_{88} \end{array}. \tag{7}$$

The associated toric diagram can be shifted in the (1, 0) direction as illustrated in Fig. 1(a) such that the new corresponding Newton polynomial takes the form,

$$\begin{aligned}P(x, y) = \bar{p}_1 \cdot \Big[&\delta_{(-1,0)} \frac{1}{x} + \delta_{(1,-2)} \frac{x}{y^2} + \delta_{(1,2)} x y^2 \\ &+ \delta_{(0,-1)} \frac{1}{y} + \delta_{(0,1)} y + \delta_{(1,-1)} \frac{x}{y} + \delta_{(1,1)} x y \\ &+ \delta_{(1,0)} x + H\Big],\end{aligned} \tag{8}$$

where the reference perfect matching weight $\bar{p}_1 = e_{11}^{+} e_{22}^{+} e_{33}^{+} e_{44}^{+} e_{55}^{+} e_{66}^{+} e_{77}^{+} e_{88}^{+}$ has been factored out. This allows

us to identify the coefficients with Casimir loops $\delta_{(n_x,n_y)}$, which correspond to points (n_x, n_y) in the toric diagram in Fig. 1(a). Additionally, we obtain the constant term H, which corresponds to the Hamiltonian of the dimer integrable system that can be expressed as a sum over all 1-loops, $H = \sum_{u=1}^{12} \gamma_u$.

The 1-loops $\gamma_{1,\ldots,12}$ and the Casimir loops $\delta_{(n_x,n_y)}$ can be expressed in terms of zigzag paths $z_{1,\ldots,8}$,

$$
\begin{aligned}
z_1 &= (e_{14}^{+} e_{44}^{-} e_{46}^{+} e_{66}^{-} e_{67}^{+} e_{77}^{-} e_{71}^{+} e_{11}^{-}),\\
z_2 &= (e_{23}^{+} e_{33}^{-} e_{35}^{+} e_{55}^{-} e_{58}^{+} e_{88}^{-} e_{82}^{+} e_{22}^{-}),\\
z_3 &= (e_{11}^{+} e_{81}^{-} e_{88}^{+} e_{68}^{-} e_{66}^{+} e_{36}^{-} e_{33}^{+} e_{13}^{-}),\\
z_4 &= (e_{22}^{+} e_{72}^{-} e_{77}^{+} e_{57}^{-} e_{55}^{+} e_{45}^{-} e_{44}^{+} e_{24}^{-}),\\
z_5 &= (e_{13}^{+} e_{23}^{-} e_{24}^{+} e_{14}^{-}), \quad z_6 = (e_{36}^{+} e_{46}^{-} e_{45}^{+} e_{35}^{-}),\\
z_7 &= (e_{57}^{+} e_{67}^{-} e_{68}^{+} e_{58}^{-}), \quad z_8 = (e_{72}^{+} e_{82}^{-} e_{81}^{+} e_{71}^{-}),
\end{aligned}
\tag{9}
$$

and the face loops $f_{1,\ldots,8}$,

$$
\begin{aligned}
f_1 &= (e_{57}^{+} e_{77}^{-} e_{71}^{+} e_{81}^{-} e_{88}^{+} e_{58}^{-}),\\
f_2 &= (e_{68}^{+} e_{88}^{-} e_{82}^{+} e_{72}^{-} e_{77}^{+} e_{67}^{-}),\\
f_3 &= (e_{45}^{+} e_{55}^{-} e_{58}^{+} e_{68}^{-} e_{66}^{+} e_{46}^{-}),\\
f_4 &= (e_{36}^{+} e_{66}^{-} e_{67}^{+} e_{57}^{-} e_{55}^{+} e_{35}^{-}),\\
f_5 &= (e_{24}^{+} e_{44}^{-} e_{46}^{+} e_{36}^{-} e_{33}^{+} e_{23}^{-}),\\
f_6 &= (e_{13}^{+} e_{33}^{-} e_{35}^{+} e_{45}^{-} e_{44}^{+} e_{14}^{-}),\\
f_7 &= (e_{11}^{+} e_{71}^{-} e_{72}^{+} e_{22}^{-} e_{23}^{+} e_{13}^{-}),\\
f_8 &= (e_{22}^{+} e_{82}^{-} e_{81}^{+} e_{11}^{-} e_{14}^{+} e_{24}^{-}),
\end{aligned}
\tag{10}
$$

of the dimer model. The face loops are the cluster variables of the quiver associated to the dimer model. The zigzag paths and face loops form the following relations:

$$
\begin{aligned}
f_1 f_2 &= z_7 z_8^{-1}, \qquad f_3 f_4 = z_6 z_7^{-1},\\
f_5 f_6 &= z_5 z_6^{-1}, \qquad f_7 f_8 = z_5^{-1} z_8,\\
f_1 f_3 f_5 f_7 &= z_3 z_4^{-1}, \qquad f_2 f_4 f_6 f_8 = z_4 z_3^{-1},\\
f_2 f_3 f_6 f_7 &= z_1^{-1} z_2, \qquad f_1 f_4 f_5 f_8 = z_1 z_2^{-1}.
\end{aligned}
\tag{11}
$$

We note here that there are 2 degrees of freedom corresponding to the pair of canonical variables e^P and e^Q, which allows us to write the face loops as follows:

$$
\begin{aligned}
f_1 &= e^{P} z_1^{1/2} z_2^{-1/2} z_7^{1/2} z_8^{-1/2},\\
f_2 &= e^{-P} z_1^{-1/2} z_2^{1/2} z_7^{1/2} z_8^{-1/2},\\
f_3 &= e^{Q} z_1^{-1/2} z_2^{1/2} z_6^{1/2} z_7^{-1/2},\\
f_4 &= e^{-Q} z_1^{1/2} z_2^{-1/2} z_6^{1/2} z_7^{-1/2},\\
f_5 &= e^{-P} z_3^{1/2} z_4^{-1/2} z_5^{1/2} z_6^{-1/2},\\
f_6 &= e^{P} z_3^{-1/2} z_4^{1/2} z_5^{1/2} z_6^{-1/2},\\
f_7 &= e^{-Q} z_3^{1/2} z_4^{-1/2} z_5^{-1/2} z_8^{1/2},\\
f_8 &= e^{Q} z_3^{-1/2} z_4^{1/2} z_5^{-1/2} z_8^{1/2},
\end{aligned}
\tag{12}
$$

where $z_1 z_2 z_3 z_4 z_5 z_6 z_7 z_8 = 1$.

In terms of these zigzag paths and face loops, the 1-loops $\gamma_{1,\ldots,12}$ can be expressed as

$$
\begin{aligned}
&\gamma_1 = z_1 z_8 f_2, \quad \gamma_2 = z_1 z_8 f_2 f_3, \quad \gamma_3 = z_1 z_8 f_1 f_2 f_3,\\
&\gamma_4 = z_1 z_8 f_2 f_3 f_6, \quad \gamma_5 = z_1 z_8 f_1 f_2 f_3 f_6,\\
&\gamma_6 = z_1 z_8 f_1 f_2 f_3 f_4 f_6, \quad \gamma_7 = z_1 z_8 f_1 f_2 f_3 f_6 f_7,\\
&\gamma_8 = z_1 z_8 f_1 f_2 f_3 f_4 f_6 f_7, \quad \gamma_9 = z_1 z_8 f_1 f_2^2 f_3 f_4 f_6 f_7,\\
&\gamma_{10} = z_1 z_8 f_1 f_2 f_3 f_4 f_5 f_6 f_7, \quad \gamma_{11} = z_1 z_8 f_1 f_2^2 f_3 f_4 f_5 f_6 f_7,\\
&\gamma_{12} = z_1 z_8 f_1 f_2^2 f_3^2 f_4 f_5 f_6 f_7,
\end{aligned}
\tag{13}
$$

and the Casimir loops $\delta_{(n_x,n_y)}$ can be expressed as

$$
\begin{aligned}
&\delta_{(1,-2)} = z_3^{-1} z_4^{-1}, \qquad \delta_{(1,2)} = z_1 z_2, \qquad \delta_{(-1,0)} = 1,\\
&\delta^1_{(0,-1)} = z_3^{-1}, \qquad \delta^2_{(0,-1)} = z_4^{-1},\\
&\delta^1_{(0,1)} = z_1, \qquad \delta^2_{(0,1)} = z_2,\\
&\delta^1_{(1,-1)} = z_3^{-1} z_4^{-1} z_5^{-1}, \qquad \delta^2_{(1,-1)} = z_3^{-1} z_4^{-1} z_6^{-1},\\
&\delta^3_{(1,-1)} = z_3^{-1} z_4^{-1} z_7^{-1}, \qquad \delta^4_{(1,-1)} = z_3^{-1} z_4^{-1} z_8^{-1},\\
&\delta^1_{(1,1)} = z_1 z_2 z_5, \qquad \delta^2_{(1,1)} = z_1 z_2 z_6,\\
&\delta^3_{(1,1)} = z_1 z_2 z_7, \qquad \delta^4_{(1,1)} = z_1 z_2 z_8,\\
&\delta^1_{(1,0)} = z_1 z_2 z_5 z_6, \qquad \delta^2_{(1,0)} = z_1 z_2 z_6 z_7,\\
&\delta^3_{(1,0)} = z_1 z_2 z_5 z_7, \qquad \delta^4_{(1,0)} = z_1 z_2 z_5 z_8,\\
&\delta^5_{(1,0)} = z_1 z_2 z_6 z_8, \qquad \delta^6_{(1,0)} = z_1 z_2 z_7 z_8.
\end{aligned}
\tag{14}
$$

Like perfect matchings, multiple Casimir loops can correspond to the same point (n_x, n_y) in the toric diagram in Fig. 1(a) and therefore can be combined as follows:

$$\begin{aligned}
\delta_{(0,-1)} &= \delta^1_{(0,-1)} + \delta^2_{(0,-1)} = z_3^{-1} + z_4^{-1},\\
\delta_{(1,-1)} &= \delta^1_{(1,-1)} + \delta^2_{(1,-1)} + \delta^3_{(1,-1)} + \delta^4_{(1,-1)} = z_3^{-1} z_4^{-1}(z_5^{-1} + z_6^{-1} + z_7^{-1} + z_8^{-1}),\\
\delta_{(1,0)} &= \delta^1_{(1,0)} + \delta^2_{(1,0)} + \delta^3_{(1,0)} + \delta^4_{(1,0)} + \delta^5_{(1,0)} + \delta^6_{(1,0)},\\
&= z_1 z_2 (z_5 z_6 + z_5 z_7 + z_5 z_8 + z_6 z_7 + z_6 z_8 + z_7 z_8),\\
\delta_{(1,1)} &= \delta^1_{(1,1)} + \delta^2_{(1,1)} + \delta^3_{(1,1)} + \delta^4_{(1,1)} = z_1 z_2 (z_5 + z_6 + z_7 + z_8),\\
\delta_{(0,1)} &= \delta^1_{(0,1)} + \delta^2_{(0,1)} = z_1 + z_2.
\end{aligned} \tag{15}$$

The zero locus of the Newton polynomial in (8) gives the spectral curve of the dimer integrable system for model 2,

$$\begin{aligned}
\Sigma: &\left(\frac{z_5}{y}+1\right)\left(\frac{z_6}{y}+1\right)\left(\frac{z_7}{y}+1\right)\left(\frac{z_8}{y}+1\right) z_1 z_2 x y^2\\
&+\left(\frac{1}{z_3}+\frac{1}{z_4}\right)\frac{1}{y} + (z_1+z_2)y + \frac{1}{x} + H = 0.
\end{aligned} \tag{16}$$

Model 4a: $\mathcal{C}/\mathbb{Z}_2 \times \mathbb{Z}_2$ (1, 0, 0, 1)(0, 1, 1, 0): The dimer model corresponding to the abelian orbifold of the form $\mathcal{C}/\mathbb{Z}_2 \times \mathbb{Z}_2$ with orbifold action (1, 0, 0, 1)(0, 1, 1, 0) is shown in Fig. 2(b). The corresponding Kasteleyn matrix is given by

$$K = \left(\begin{array}{c|cccc}
 & b_1 & b_2 & b_3 & b_4\\
\hline
w_1 & e_{11} & e_{12}x^{-1} & e_{13}y^{-1} & e_{14}x^{-1}y^{-1}\\
w_2 & e_{21} & e_{22} & e_{23}y^{-1} & e_{24}y^{-1}\\
w_3 & e_{31} & e_{32}x^{-1} & e_{33} & e_{34}x^{-1}\\
w_4 & e_{41} & e_{42} & e_{43} & e_{44}
\end{array}\right). \tag{17}$$

When we shift the toric diagram in the (1, 1) direction resulting in the toric diagram in Fig. 2(a), the corresponding Newton polynomial becomes

$$\begin{aligned}
P(x,y) = \bar{u}_1 \cdot \Big[&\delta_{(-1,-1)}\frac{1}{xy} + \delta_{(-1,1)}\frac{y}{x} + \delta_{(1,-1)}\frac{x}{y}\\
&+ \delta_{(1,1)}xy + \delta_{(-1,0)}\frac{1}{x} + \delta_{(0,-1)}\frac{1}{y} + \delta_{(1,0)}x\\
&+ \delta_{(0,1)}y + H\Big],
\end{aligned} \tag{18}$$

where the reference perfect matching weight $\bar{u}_1 = e_{14}^+ e_{21}^+ e_{32}^+ e_{43}^+$ has been factored out in order for the coefficients to become Casimir loops $\delta_{(n_x,n_y)}$. These correspond to points in the toric diagram in Fig. 2(a). We also obtain the Hamiltonian H, which can be expressed as a sum over all 1-loops, $H = \sum_{u=1}^{12} \gamma_u$.

The 1-loops $\gamma_{1,\ldots,12}$ and the Casimir loops $\delta_{(n_x,n_y)}$ can be expressed in terms of zigzag paths $z_{1,\ldots,8}$,

$$\begin{aligned}
z_1 &= (e_{11}^+ e_{21}^- e_{22}^+ e_{12}^-), & z_2 &= (e_{32}^+ e_{42}^- e_{41}^+ e_{31}^-),\\
z_3 &= (e_{33}^+ e_{43}^- e_{44}^+ e_{34}^-), & z_4 &= (e_{14}^+ e_{24}^- e_{23}^+ e_{13}^-),\\
z_5 &= (e_{13}^+ e_{33}^- e_{31}^+ e_{11}^-), & z_6 &= (e_{21}^+ e_{41}^- e_{43}^+ e_{23}^-),\\
z_7 &= (e_{24}^+ e_{44}^- e_{42}^+ e_{22}^-), & z_8 &= (e_{12}^+ e_{32}^- e_{34}^+ e_{14}^-),
\end{aligned} \tag{19}$$

and the face loops $f_{1,\ldots,8}$,

$$\begin{aligned}
f_1 &= (e_{22}^+ e_{42}^- e_{41}^+ e_{21}^-), & f_2 &= (e_{43}^+ e_{33}^- e_{31}^+ e_{41}^-),\\
f_3 &= (e_{44}^+ e_{24}^- e_{23}^+ e_{43}^-), & f_4 &= (e_{21}^+ e_{11}^- e_{13}^+ e_{23}^-),\\
f_5 &= (e_{33}^+ e_{13}^- e_{14}^+ e_{34}^-), & f_6 &= (e_{12}^+ e_{22}^- e_{24}^+ e_{14}^-),\\
f_7 &= (e_{11}^+ e_{31}^- e_{32}^+ e_{12}^-), & f_8 &= (e_{34}^+ e_{44}^- e_{42}^+ e_{32}^-).
\end{aligned} \tag{20}$$

The face loops and zigzag paths form the following relations:

$$\begin{aligned}
f_1 f_7 &= z_1 z_2, & f_2 f_8 &= z_2^{-1} z_3^{-1},\\
f_3 f_5 &= z_3 z_4, & f_4 f_6 &= z_1^{-1} z_4^{-1},\\
f_2 f_4 &= z_5 z_6, & f_1 f_3 &= z_6^{-1} z_7^{-1},\\
f_6 f_8 &= z_7 z_8, & f_5 f_7 &= z_5^{-1} z_8^{-1}.
\end{aligned} \tag{21}$$

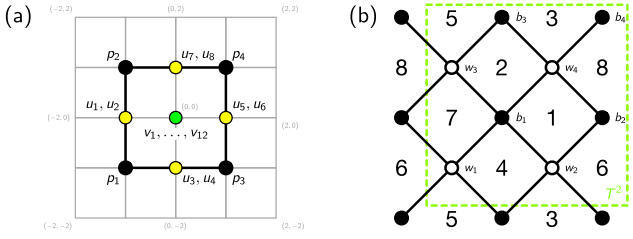

FIG. 2. (a) The toric diagram and (b) the dimer model for $\mathcal{C}/\mathbb{Z}_2 \times \mathbb{Z}_2$ (1, 0, 0, 1)(0, 1, 1, 0) [model 4a]. Points in the toric diagram are labelled by corresponding perfect matchings in the dimer model.

Here, we note that there are 2 degrees of freedom corresponding to the pair of canonical variables e^P and e^Q, which allows us to express the face loops as follows:

$$\begin{aligned} f_1 &= e^Q, \qquad f_2 = e^P, \\ f_3 &= e^{-Q} z_6^{-1} z_7^{-1}, \qquad f_4 = e^{-P} z_5 z_6, \\ f_5 &= e^Q z_3 z_4 z_6 z_7, \qquad f_6 = e^P z_1^{-1} z_4^{-1} z_5^{-1} z_6^{-1}, \\ f_7 &= e^{-Q} z_1 z_2, \qquad f_8 = e^{-P} z_2^{-1} z_3^{-1}, \end{aligned} \tag{22}$$

where $z_1 z_2 z_3 z_4 z_5 z_6 z_7 z_8 = 1$.

In terms of the face loops and the zigzag paths, we can express the 1-loops $\gamma_{1,\ldots,12}$ as

$$\begin{aligned} \gamma_1 &= z_1 f_6, \qquad \gamma_2 = z_1 f_3 f_6, \qquad \gamma_3 = z_1 f_3 f_6 f_8, \\ \gamma_4 &= z_1 f_3 f_4 f_6, \qquad \gamma_5 = z_1 f_3 f_4 f_6 f_8, \\ \gamma_6 &= z_1 f_1 f_3 f_4 f_6 f_8, \qquad \gamma_7 = z_1 f_3 f_4 f_5 f_6 f_8, \\ \gamma_8 &= z_1 f_1 f_3 f_4 f_5 f_6 f_8, \qquad \gamma_9 = z_1 f_1 f_3 f_4 f_5 f_6^2 f_8, \\ \gamma_{10} &= z_1 f_1 f_2 f_3 f_4 f_5 f_6 f_8, \qquad \gamma_{11} = z_1 f_1 f_2 f_3 f_4 f_5 f_6^2 f_8, \\ \gamma_{12} &= z_1 f_1 f_2 f_3^2 f_4 f_5 f_6^2 f_8, \end{aligned} \tag{23}$$

and the Casimir loops $\delta^a_{(n_x,n_y)}$ as

$$\begin{aligned} \delta_{(-1,-1)} &= z_6^{-1}, \quad \delta_{(-1,1)} = z_8, \\ \delta_{(1,-1)} &= z_2^{-1} z_4^{-1} z_6^{-1}, \quad \delta_{(1,1)} = z_1 z_3 z_8, \\ \delta^1_{(-1,0)} &= 1, \quad \delta^2_{(-1,0)} = z_6^{-1} z_8, \\ \delta^1_{(0,-1)} &= z_2^{-1} z_6^{-1}, \quad \delta^2_{(0,-1)} = z_4^{-1} z_6^{-1}, \\ \delta^1_{(1,0)} &= z_1 z_3 z_7 z_8, \quad \delta^2_{(1,0)} = z_2^{-1} z_4^{-1} z_6^{-1} z_7^{-1}, \\ \delta^1_{(0,1)} &= z_1 z_8, \quad \delta^2_{(0,1)} = z_3 z_8, \end{aligned} \tag{24}$$

where Casimir loops corresponding to the same point in the toric diagram in Fig. 2(a) can be combined as follows:

$$\begin{aligned} \delta_{(-1,0)} &= \delta^1_{(-1,0)} + \delta^2_{(-1,0)} = 1 + z_6^{-1} z_8, \\ \delta_{(0,-1)} &= \delta^1_{(0,-1)} + \delta^2_{(0,-1)} = z_2^{-1} z_6^{-1} + z_4^{-1} z_6^{-1}, \\ \delta_{(1,0)} &= \delta^1_{(1,0)} + \delta^2_{(1,0)} = z_1 z_3 z_7 z_8 + z_2^{-1} z_4^{-1} z_6^{-1} z_7^{-1}, \\ \delta_{(0,1)} &= \delta^1_{(0,1)} + \delta^2_{(0,1)} = z_1 z_8 + z_3 z_8. \end{aligned} \tag{25}$$

The spectral curve of the dimer integrable system for model 4a is given by the zero locus of the Newton polynomial in (18)

$$\begin{aligned} \Sigma: &\left(\frac{1}{y} + z_6\right)\left(\frac{1}{y} + z_8\right)\frac{y}{z_6 x} + \left(\frac{1}{z_2} + \frac{1}{z_4}\right)\frac{1}{z_6 y} \\ &+ \left(\frac{1}{y} + \frac{1}{z_5}\right)\left(\frac{1}{y} + \frac{1}{z_7}\right)\frac{xy}{z_2 z_4 z_6} + (z_1 + z_3) z_8 y \\ &+ H = 0. \end{aligned} \tag{26}$$

Birational equivalence. Let us refer to the Newton polynomial in (8) and the spectral curve in (16) for model 2 as $P^{(2)}(x,y)$ and $\Sigma^{(2)}$, respectively, in order to distinguish them clearly from the Newton polynomial in (18) and the spectral curve in (26) for model 4a, which we denote by $P^{(4a)}(x,y)$ and $\Sigma^{(4a)}$, respectively. The following birational transformation:

$$\varphi_A : (x,y) \mapsto \left(\left(1 + \frac{1}{y}\right)^2 xy, y\right), \tag{27}$$

acts on the Newton polynomial with all perfect matching weights set to 1, yielding the identification,

$$\varphi_A P^{(4a)}(x,y) = P^{(2)}(x,y). \tag{28}$$

This birational transformation relates the toric varieties associated to models 2 and 4a.

Under a refined version of the birational transformation in (27), given by

$$\varphi_A : (x,y) \mapsto \left(\left(z_6^{(4a)} + \frac{1}{y}\right)\left(z_8^{(4a)} + \frac{1}{y}\right)\frac{y}{z_6^{(4a)}} x, y\right), \tag{29}$$

with $A(y) = (z_6^{(4a)} + \frac{1}{y})(z_8^{(4a)} + \frac{1}{y})\frac{y}{z_6^{(4a)}}$, we discover that the spectral curve $\Sigma^{(4a)}$ in (26) is mapped to $\Sigma^{(2)}$ in (16),

$$\varphi_A \Sigma^{(4a)} = \Sigma^{(2)}. \tag{30}$$

Under this identification, the zigzag loops satisfy

$$\begin{aligned} &z_1^{(4a)} z_8^{(4a)} = z_1^{(2)}, \quad z_3^{(4a)} z_8^{(4a)} = z_2^{(2)}, \quad z_5^{(4a)} = z_5^{(2)}, \\ &z_2^{(4a)} z_6^{(4a)} = z_4^{(2)}, \quad z_4^{(4a)} z_6^{(4a)} = z_3^{(2)}, \quad z_6^{(4a)} = (z_6^{(2)})^{-1}, \\ &z_7^{(4a)} = z_7^{(2)}, \quad z_8^{(4a)} = (z_8^{(2)})^{-1}, \end{aligned} \tag{31}$$

and the face loops between the two dimer models are identified to each other as follows:

$$\begin{aligned} &f_8^{(4a)} = f_1^{(2)}, \quad f_6^{(4a)} = f_2^{(2)}, \quad f_3^{(4a)} = f_3^{(2)}, \\ &f_1^{(4a)} = f_4^{(2)}, \quad f_2^{(4a)} = f_5^{(2)}, \quad f_4^{(4a)} = f_6^{(2)}, \\ &f_5^{(4a)} = f_7^{(2)}, \quad f_7^{(4a)} = f_8^{(2)}. \end{aligned} \tag{32}$$

Moreover, the 1-loops of the two integrable systems also obey

$$\gamma_u^{(4a)} = \gamma_u^{(2)}, \tag{33}$$

for all $u = 1, \ldots, 12$. This implies that the two Hamiltonians of the dimer integrable systems are identical under the birational transformation in (29),

$$H^{(4a)} = H^{(2)}. \tag{34}$$

By identifying (12) with (22), we also obtain the following canonical transformation:

$$\begin{aligned} e^{Q^{(4a)}} &= e^{-Q^{(2)}}(z_1^{(2)} z_6^{(2)})^{1/2}(z_2^{(2)} z_7^{(2)})^{-1/2}, \\ e^{P^{(4a)}} &= e^{-P^{(2)}}(z_3^{(2)} z_5^{(2)})^{1/2}(z_4^{(2)} z_6^{(2)})^{-1/2}. \end{aligned} \tag{35}$$

Accordingly, we can summarize that the birational transformation in (29) identifies the Casimirs and the Hamiltonians as well as the spectral curve and the Poisson structure formed by the cluster variables of the two dimer integrable systems. We thus identify the two integrable systems corresponding to model 2 and 4a to be birationally equivalent under (29).

In general, we conjecture that whenever two toric Calabi-Yau 3-folds and their corresponding toric varieties are related by a birational transformation, there exists a pair of associated dimer models whose respective dimer integrable systems are birationally equivalent. Here, we define birational equivalence as an identification of the Casimirs and the Hamiltonians as well as the spectral curve and the Poisson structure formed by the cluster variables of the two dimer integrable systems. We anticipate that this observation extends also to the corresponding quantum integrable systems. Moreover, we can report here that this observation has been confirmed for dimer models corresponding to more general toric Calabi-Yau 3-folds including those with toric diagrams that are not reflexive polygons. We also note here that the birational transformations identifying zigzag loops and face loops between two different dimer models have interesting interpretations as deformations of the associated $4d$ $\mathcal{N}=1$ gauge theories [14,15,25,50,51]. We also identify the birational transformations of the toric diagrams to be related to Hanany-Witten moves in the dual (p,q)-web diagrams associated to $5d$ $\mathcal{N}=1$ gauge theories [35,50–53]. This connection also paves the way to further understand generalized toric polytopes (GTP) [35,50–53] that appear in the study of $5d$ $\mathcal{N}=1$ gauge theories. We plan to report further on these findings in the near future.

Acknowledgments. The authors would like to thank J. Bao, S. Franco, D. Ghim, Y.-H. He, S. Jeong, K. Lee, and M. Yamazaki for discussions. R.-K. S. is supported by an Outstanding Young Scientist Grant (RS-2025-00516583) of the National Research Foundation of Korea (NRF). He is also partly supported by the BK21 Program ("Next Generation Education Program for Mathematical Sciences," 4299990414089) funded by the Ministry of Education in Korea and the National Research Foundation of Korea (NRF). N. L. is supported by the Institute of Basic Science (IBS-R003-D1).

Data availability

No data were created or analyzed in this study.

[1] S. Mori, Projective manifolds with ample tangent bundles, Ann. Math. **110**, 593 (1979).
[2] S. Mori, Threefolds whose canonical bundles are not numerically effective, Ann. Math. **116**, 133 (1982).
[3] S. Mori, Flip theorem and the existence of minimal models for 3-folds, J. Am. Math. Soc. **1**, 117 (1988).
[4] Y. Kawamata, Pluricanonical systems on minimal algebraic varieties, Inventiones Mathematicae **79**, 567 (1985).
[5] J. Kollár, Y. Miyaoka, and S. Mori, Rationally connected varieties, J. Algebr. Geom. **1**, 429 (1992), https://zbmath.org/0780.14026.
[6] J. Kollár and S. Mori, *Birational Geometry of Algebraic Varieties*, Cambridge Tracts in Mathematics (Cambridge University Press, Cambridge, England, 1998).
[7] C. Birkar, P. Cascini, C. Hacon, and J. McKernan, Existence of minimal models for varieties of log general type, J. Am. Math. Soc. **23**, 405 (2010).
[8] M. Akhtar, T. Coates, S. Galkin, A. M. Kasprzyk *et al.*, Minkowski polynomials and mutations, SIGMA **8**, 094 (2012).
[9] M. Gross, P. Hacking, and S. Keel, Birational geometry of cluster algebras, arXiv:1309.2573.
[10] T. Coates, A. Corti, S. Galkin, and A. Kasprzyk, Quantum periods for 3–dimensional fano manifolds, Geom. Topol. **20**, 103 (2016).
[11] A. Kasprzyk, B. Nill, and T. Prince, Minimality and mutation-equivalence of polygons, in *Forum of Mathematics, Sigma* (Cambridge University Press, Cambridge, England, 2017), Vol. 5, p. e18.
[12] T. Coates, A. M. Kasprzyk, G. Pitton, and K. Tveiten, Maximally mutable laurent polynomials, Proc. R. Soc. A **477**, 20210584 (2021).
[13] T. Coates, L. Heuberger, and A. M. Kasprzyk, Mirror symmetry, laurent inversion and the classification of $\mathbb{Q}$-fano threefolds, arXiv:2210.07328.
[14] D. Ghim, M. Kho, and R.-K. Seong, Combinatorial and algebraic mutations of toric Fano 3-folds and mass deformations of 2d(0,2) quiver gauge theories, Phys. Rev. D **110**, 086001 (2024).
[15] D. Ghim, M. Kho, and R.-K. Seong, Birational transformations and 2d (0, 2) quiver gauge theories beyond toric Fano 3-folds, J. High Energy Phys. 06 (2025) 032.
[16] R. Kenyon, Local statistics of lattice dimers, Ann. l'Inst. Henri Poincare (B) Probab. Stat. **33**, 591 (1997).

[17] R. Kenyon, An introduction to the dimer model, arXiv:math/0310326.
[18] A. Hanany and K. D. Kennaway, Dimer models and toric diagrams, arXiv:hep-th/0503149.
[19] S. Franco, A. Hanany, K. D. Kennaway, D. Vegh, and B. Wecht, Brane dimers and quiver gauge theories, J. High Energy Phys. 01 (2006) 096.
[20] S. Franco, A. Hanany, D. Martelli, J. Sparks, D. Vegh, and B. Wecht, Gauge theories from toric geometry and brane tilings, J. High Energy Phys. 01 (2006) 128.
[21] I. R. Klebanov and E. Witten, Superconformal field theory on three-branes at a Calabi-Yau singularity, Nucl. Phys. **B536**, 199 (1998).
[22] S. Gubser, N. Nekrasov, and S. Shatashvili, Generalized conifolds and 4-dimensional $N = 1$ superconformal field theory, J. High Energy Phys. 05 (1999) 003.
[23] M. Bianchi, S. Cremonesi, A. Hanany, J. F. Morales, D. Ricci Pacifici, and R.-K. Seong, Mass-deformed brane tilings, J. High Energy Phys. 10 (2014) 027.
[24] S. Franco, D. Ghim, G. P. Goulas, and R.-K. Seong, Mass deformations of brane brick models, J. High Energy Phys. 09 (2023) 176.
[25] A. Higashitani, Y. Nakajima *et al.*, Deformations of dimer models, SIGMA **18**, 030 (2022).
[26] W. Fulton, *Introduction to Toric Varieties*, No. 131 (Princeton University Press, Princeton, NJ, 1993).
[27] N. C. Leung and C. Vafa, Branes and toric geometry, Adv. Theor. Math. Phys. **2**, 91 (1998).
[28] P. Kasteleyn, *Graph theory and crystal physics, Graph Theory and Theoretical Physics* (Academic Press, London, 1967), pp. 43–110.
[29] A. B. Goncharov and R. Kenyon, Dimers and cluster integrable systems, arXiv:1107.5588.
[30] R. Eager, S. Franco, and K. Schaeffer, Dimer models and integrable systems, J. High Energy Phys. 06 (2012) 106.
[31] M. Bershtein, P. Gavrylenko, and A. Marshakov, Cluster integrable systems, q-Painlevé equations and their quantization, J. High Energy Phys. 02 (2018) 077.
[32] A. Marshakov and M. Semenyakin, Cluster integrable systems and spin chains, J. High Energy Phys. 10 (2019) 100.
[33] M.-x. Huang, Y. Sugimoto, and X. Wang, Quantum periods and spectra in dimer models and Calabi-Yau geometries, J. High Energy Phys. 09 (2020) 168.
[34] N. Lee, New dimer integrable systems and defects in five dimensional gauge theory, J. High Energy Phys. 12 (2024) 050.
[35] K. Lee and N. Lee, Dimers for type D relativistic Toda model, J. High Energy Phys. 09 (2024) 198.
[36] M. R. Douglas, B. R. Greene, and D. R. Morrison, Orbifold resolution by D-branes, Nucl. Phys. **B506**, 84 (1997).
[37] M. R. Douglas and G. W. Moore, D-branes, quivers, and ALE instantons, arXiv:hep-th/9603167.
[38] B. Feng, A. Hanany, and Y.-H. He, D-brane gauge theories from toric singularities and toric duality, Nucl. Phys. **B595**, 165 (2001).
[39] B. Feng, A. Hanany, and Y.-H. He, Phase structure of D-brane gauge theories and toric duality, J. High Energy Phys. 08 (2001) 040.
[40] K. Hori, A. Iqbal, and C. Vafa, D-branes and mirror symmetry, arXiv:hep-th/0005247.
[41] K. Hori and C. Vafa, Mirror symmetry, arXiv:hep-th/0002222.
[42] B. Feng, Y.-H. He, K. D. Kennaway, and C. Vafa, Dimer models from mirror symmetry and quivering amoebae, Adv. Theor. Math. Phys. **12**, 489 (2008).
[43] J. Davey, A. Hanany, and R.-K. Seong, Counting orbifolds, J. High Energy Phys. 06 (2010) 010.
[44] A. Hanany and R.-K. Seong, Symmetries of Abelian orbifolds, J. High Energy Phys. 01 (2011) 027.
[45] A. Hanany and R.-K. Seong, Brane tilings and reflexive polygons, Fortschr. Phys. **60**, 695 (2012).
[46] B. Feng, S. Franco, A. Hanany, and Y.-H. He, UnHiggsing the del Pezzo, J. High Energy Phys. 08 (2003) 058.
[47] E. Witten, Phases of $N = 2$ theories in two-dimensions, Nucl. Phys. **B403**, 159 (1993).
[48] V. Jejjala, S. Ramgoolam, and D. Rodriguez-Gomez, Toric CFTs, permutation triples and Belyi pairs, J. High Energy Phys. 03 (2011) 065.
[49] A. Hanany, V. Jejjala, S. Ramgoolam, and R.-K. Seong, Consistency and derangements in brane tilings, J. Phys. A **49**, 355401 (2016).
[50] S. Franco and R.-K. Seong, Twin theories, polytope mutations and quivers for GTPs, J. High Energy Phys. 07 (2023) 034.
[51] G. Arias-Tamargo, S. Franco, and D. Rodríguez-Gómez, The geometry of GTPs and 5d SCFTs, J. High Energy Phys. 07 (2024) 159.
[52] S. Franco and D. Rodriguez-Gomez, Quiver tails and brane webs, J. High Energy Phys. 10 (2024) 118.
[53] I. Carreño Bolla, S. Franco, and D. Rodríguez-Gómez, The 5d tangram: Brane webs, 7-branes and primitive T-cones, J. High Energy Phys. 05 (2025) 175.